Cell Reports

The neural correlates of arousal: Ventral posterolateral nucleus-global transient co-activation

Graphical abstract

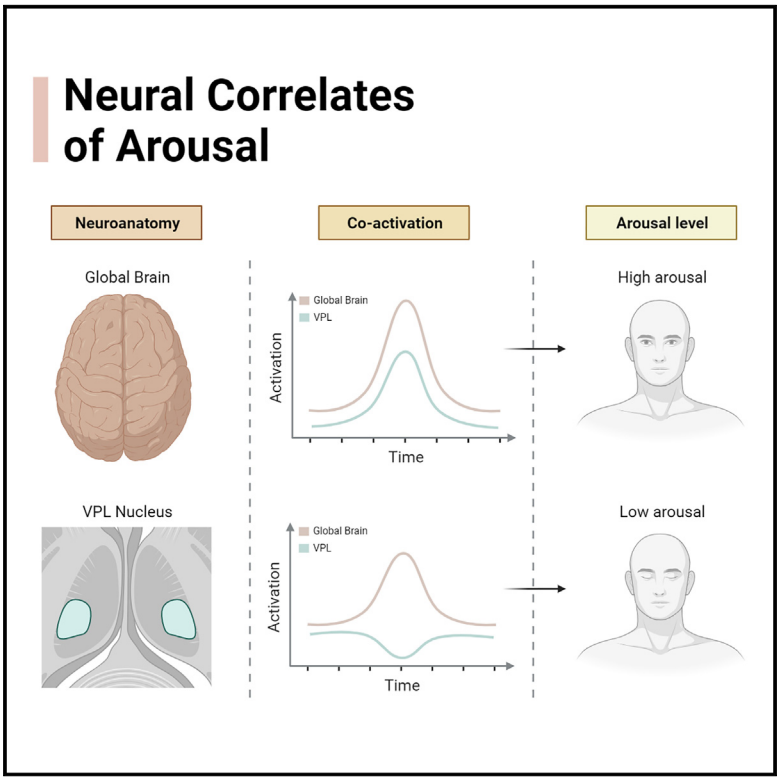

Highlights

- Co-activation of VPL and global brain is elevated in wakefulness and unresponsive wakefulness
- VPL activity is reduced in low arousal states compared to global brain activity
- Co-activation of VPL and global transient signal is related to arousal rather than awareness
- VPL might attain co-activation with global cortex via sensory-motor areas to modulate arousal

Authors

Junrong Han, Qiuyou Xie, Xuehai Wu, ..., Ying Mao, Sheng He, Pengmin Qin

Correspondence

maoying@fudan.edu.cn (Y.M.), hes@ibp.ac.cn (S.H.), qin.pengmin@m.scnu.edu.cn (P.Q.)

In brief

Han et al. employed multi-center fMRI data to dissociate the components of consciousness, arousal, and awareness. By comparing co-activation of spontaneous global brain signal across conditions, they demonstrate that transient co-activation of the ventral posterolateral nucleus and global signal is predominantly associated with arousal rather than awareness.

Han et al., 2024, Cell Reports *43*, 113633
January 23, 2024
https://doi.org/10.1016/j.celrep.2023.113633

CellPress

Cell Reports

CellPress
OPEN ACCESS

Report

The neural correlates of arousal: Ventral posterolateral nucleus-global transient co-activation

Junrong Han,[1,12] Qiuyou Xie,[2,3,12] Xuehai Wu,[4,12] Zirui Huang,[5] Sean Tanabe,[5] Stuart Fogel,[6] Anthony G. Hudetz,[5] Hang Wu,[7] Georg Northoff,[8,9] Ying Mao,[4,*] Sheng He,[10,*] and Pengmin Qin[7,11,13,*]

[1]Key Laboratory of Brain, Cognition and Education Sciences, Ministry of Education, Institute for Brain Research and Rehabilitation, Guangdong Key Laboratory of Mental Health and Cognitive Science, South China Normal University, Guangzhou 510631, China
[2]Department of Rehabilitation Medicine, Zhujiang Hospital, Southern Medical University, Guangzhou 510280, Guangdong, China
[3]Joint Research Centre for Disorders of Consciousness, Guangzhou, Guangdong, China
[4]Department of Neurosurgery, Huashan Hospital, Shanghai Medical College, Fudan University, Shanghai, China
[5]Department of Anesthesiology, Center for Consciousness Science, University of Michigan, Ann Arbor, MI, USA
[6]School of Psychology, University of Ottawa, Ottawa, ON, Canada
[7]Center for Studies of Psychological Application, School of Psychology, South China Normal University, Guangzhou 510631, Guangdong, China
[8]Institute of Mental Health Research, University of Ottawa, Ottawa, ON, Canada
[9]Mental Health Centre, Zhejiang University School of Medicine, Hangzhou, China
[10]State Key Laboratory of Brain and Cognitive Science, Institute of Biophysics, Chinese Academy of Sciences, Beijing 100101, China
[11]Pazhou Lab, Guangzhou 510335, China
[12]These authors contributed equally
[13]Lead contact
*Correspondence: maoying@fudan.edu.cn (Y.M.), hes@ibp.ac.cn (S.H.), qin.pengmin@m.scnu.edu.cn (P.Q.)
https://doi.org/10.1016/j.celrep.2023.113633

SUMMARY

Arousal and awareness are two components of consciousness whose neural mechanisms remain unclear. Spontaneous peaks of global (brain-wide) blood-oxygenation-level-dependent (BOLD) signal have been found to be sensitive to changes in arousal. By contrasting BOLD signals at different arousal levels, we find decreased activation of the ventral posterolateral nucleus (VPL) during transient peaks in the global signal in low arousal and awareness states (non-rapid eye movement sleep and anesthesia) compared to wakefulness and in eyes-closed compared to eyes-open conditions in healthy awake individuals. Intriguingly, VPL-global co-activation remains high in patients with unresponsive wakefulness syndrome (UWS), who exhibit high arousal without awareness, while it reduces in rapid eye movement sleep, a state characterized by low arousal but high awareness. Furthermore, lower co-activation is found in individuals during N3 sleep compared to patients with UWS. These results demonstrate that co-activation of VPL and global activity is critical to arousal but not to awareness.

INTRODUCTION

Consciousness can be divided along two axes: awareness (i.e., subjective experience; the mental contents of consciousness) and arousal (i.e., the states of wakefulness; neurophysiological arousal).[1] By investigating these two components, researchers have observed that both slow-wave sleep and anesthesia states exhibited diminished awareness and arousal. Conversely, unresponsive wakefulness syndrome (UWS), formerly known as the vegetative state, is characterized by high arousal without awareness, while rapid eye movement (REM) sleep displays diminished arousal and high awareness (Figure 1A). Especially, a state of high arousal in patients with UWS is marked by eye opening[1] and increased neural activity of the brain stem.[2] However, despite extensive research into the neural mechanism of awareness,[3–7] a controversy remains regarding the specific interaction between arousal systems and large-scale brain activity in regulating arousal as a component of consciousness.

Nevertheless, emerging evidence indicates a potential link between arousal and brain-wide (e.g., global) spontaneous blood-oxygenation-level-dependent (BOLD) signal (global signal [GS]) fluctuations.[8–11] For instance, a study demonstrated a progressive decrease in GS amplitude, defined as the temporal standard deviation of GS time series, from morning to afternoon, suggesting a positive correlation between arousal and GS amplitude[12] (but see other studies[8,9]). Intriguingly, previous research has suggested that global spontaneous activity, in collaboration with the thalamus, could contribute to arousal. For example, the transient peaks in GS (top 16.6% GS series) during the resting state were found to be associated with the deactivation

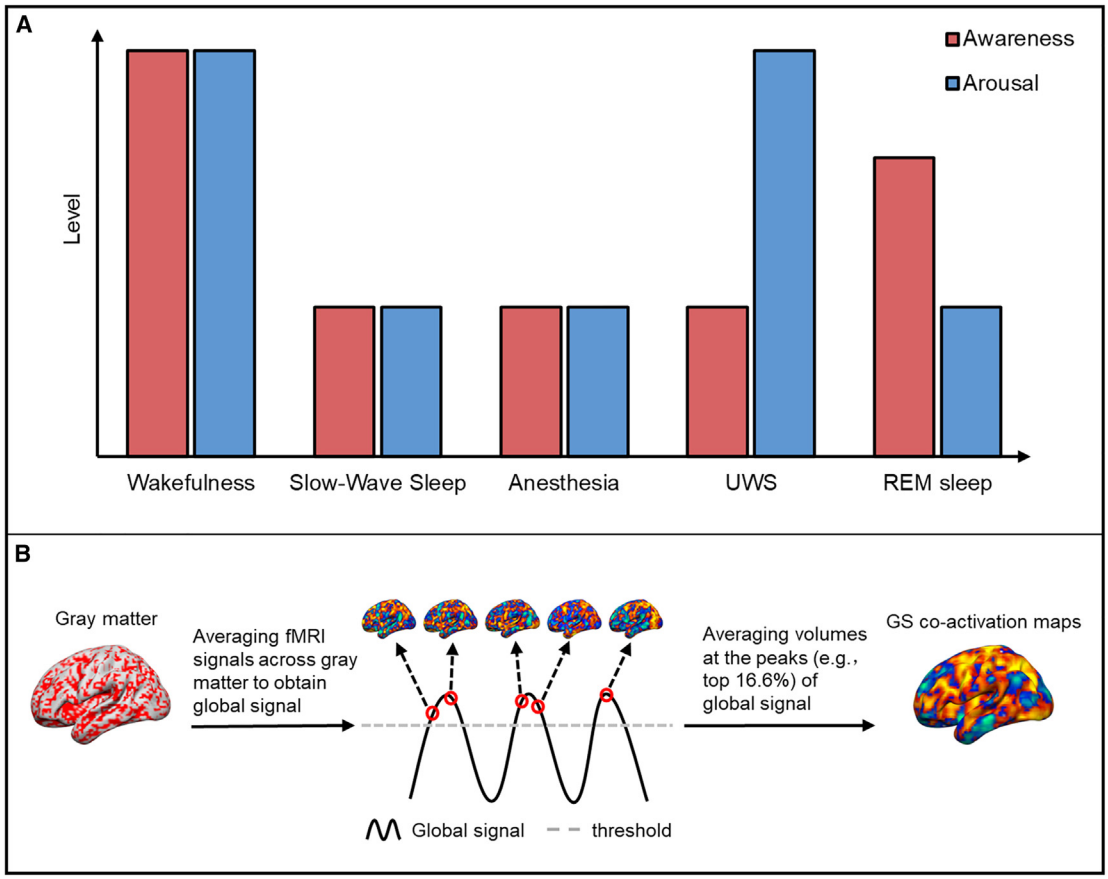

Figure 1. Arousal states and analytical methods performed in this study

(A) Schematic representation of awareness and arousal components across different consciousness states.

(B) Schematic elucidating the method employed for generating GS co-activation maps.

in the dorsal midline thalamus, indicating a momentary drop of arousal.[13] On the other hand, deep brain stimulation of the central thalamus or the central lateral thalamus induced widespread cortical activity and improved consciousness in heavily sedated macaques and patients with disorders of consciousness.[14–16] These studies collectively highlight the involvement of the dorsal midline thalamus, central thalamus, and central lateral thalamus in modulating consciousness, including both arousal and awareness. Thus, it is unlikely that these thalamic nuclei predominantly contribute to arousal but not awareness. Based on these findings, we propose the hypothesis that neural mechanisms underlying arousal may involve additional thalamic nuclei, such as sensory thalamic nuclei, which modulate global spontaneous activity and may relate to perceptual consciousness.[17–20]

To investigate the role of functional interaction between thalamic and global brain activities in relation to arousal, we analyzed multi-center resting-state fMRI datasets encompassing various arousal levels. These levels included different sleep stages, anesthesia, UWS, and wakeful resting state in healthy participants with eyes open and eyes closed (EO/EC) (Table 1). Our primary objective was to examine changes in thalamus activation during GS peaks among strongly altered arousal levels (N2 and N3 sleep and anesthesia) and slightly altered arousal levels between EO and EC conditions in healthy awake individuals. As both awareness and arousal are concurrently diminished in suppressed states like sleep and anesthesia, we aimed to dissociate these components of consciousness by analyzing additional data from patients with UWS, characterized by high arousal without evident signs of awareness, and REM sleep, characterized by low arousal but high awareness.[1]

Specifically, for all the datasets, we conducted co-activation analysis to capture momentary changes in thalamic activity during spontaneous transient peaks of the GS.[21] We first calculated the GS by averaging the *Z* score-transformed time series across all voxels within the gray matter and then selected the top 16.6% time points of the GS to represent the instantaneous peaks.[13,22] The activation maps corresponding to these GS peaks (top 16.6%) were averaged to generate the GS co-activation map[13,22] (Figure 1B). By comparing the GS co-activation in the thalamus across different arousal states, we identified the specific thalamic nucleus exhibiting differential activation by overlapping it with the atlas of human subcortical areas.

As we will show, peaks in GS were accompanied by higher activity in the ventral posterolateral nucleus (VPL), a sensory nucleus of the thalamus, only in the states of high arousal, irrespective of the level of awareness. This finding suggests that

Table 1. Detailed information for all datasets

Dataset	Site	Condition	No. of subjects	Gender (male)	Age	Total number of time points at GS peaks
Sleep	IUGM/WU	W	30	12	25.06 (±4.08)	1,254
		N2	37	15	25.30 (±4.18)	1,597
		N3	18	8	24.06 (±4.07)	734
Anesthesia	WIS/WU	W	30	–	–	1,692
		DS	23	–	–	1,289
EO/EC	BNU 1/BNU 2	EO	67	34	22.04 (±2.18)	2,613
EO/EC	BNU 1/BNU 2	EC	67	34	22.04 (±2.18)	2,613
UWS 1	SHH	BI	15	11	38.80 (±16.89)	501
UWS 1	SHH	UWS	19	14	45.84 (±12.49)	606
UWS 2	ZJH	HC	21	10	32.33 (±10.42)	887
		UWS	19	10	51.16 (±11.57)	765
REM sleep	WU	REM	7	3	23.86 (±5.08)	371
REM sleep	WU	N3	10	4	22.30 (±4.06)	412
REM sleep	WU	W	19	7	23.89 (±3.75)	792
N3 vs. UWS	N3: IUGM/WU; UWS: SHH/ZJH	N3	18	8	24.06 (±4.07)	731
N3 vs. UWS	N3: IUGM/WU; UWS: SHH/ZJH	UWS	38	24	48.50 (±12.18)	1,371

As for concerning the participants privacy, the anesthesia data from Western University (WU) only provided aggregated demographic information for all participants (total 17 participants, 13 male, age 24 ± 5), without individual details available on OpenNeuro. Therefore, descriptive statistics regarding gender and age could not be conducted for the remaining participants who did not exhibit excessive head motion in the anesthesia dataset. The demographic information for each subdataset is provided in the STAR Methods.

the co-activation between the VPL and GS is critical to arousal but not to awareness.

RESULTS

To investigate changes in the thalamic GS co-activation pattern during naturally reduced arousal states, we utilized fMRI data across wakefulness, N2-sleep, and N3-sleep stages (Table 1). A one-way ANOVA (two-tailed) was employed to compare GS co-activation across the three stages within the thalamus. The result revealed significant voxel-wise alteration within the thalamus across sleep stages (false discovery rate [FDR]-corrected $q < 0.05$) (Figure 2A).

To further explore the effect of pharmacologically induced arousal reduction on thalamus-global transient co-activation, we examined an anesthesia fMRI dataset that included wakefulness and deep sedation conditions (Table 1). Using voxel-wise independent sample t tests (two-tailed), we observed significantly higher GS co-activation in several areas of the thalamus during wakefulness compared to deep sedation (FDR-corrected $q < 0.05$) (Figure 2B).

Additionally, we investigated the impact of minor arousal reductions on thalamus-global transient co-activation using resting-state fMRI datasets from healthy participants in EO and EC states (Table 1). Voxel-wise paired t tests (two-tailed) revealed a significant decrease in GS co-activation in most of the thalamus during the EC condition compared to the EO condition (FDR-corrected $q < 0.05$) (Figure 2C).

Moreover, overlaying brain maps from GS co-activation comparisons across sleep, anesthesia, and EO/EC datasets identified several thalamic subregions. These regions exhibited disrupted instantaneous co-activation with GS peaks (i.e., thalamus-global transient co-activation) when arousal decreased (Figure 2D). Utilizing the atlas of subcortical areas,[23] we identified overlap with multiple thalamic nuclei, including left VPL (lVPL) nuclei, left anterior/inferior/lateral/medial pulvinar (PULa, PULi, PULl, PULm) nuclei, and right mediodorsolateral/mediodorsomedial (MDl/MDm) nuclei (Figure 2E). We combined the overlapped areas for left PULa, PULi, PULl, and PULm to represent the left pulvinar (lPUL) nucleus and for right MDl and MDm to represent the right mediodorsal (rMD) nucleus. Finally, the overlapped area was segmented into three nuclei, including the lVPL, lPUL, and rMD, which served as regions of interest (ROIs) for further analyses.

To elucidate global co-activation alteration among the three identified nuclei (lVPL, lPUL, rMD) during transitions between arousal states, we compared their GS co-activation across different arousal states using the sleep, anesthesia, and EO/EC fMRI datasets. ROI-based analyses involved calculating the mean GS co-activation within each nucleus and comparing them across conditions. Bayesian statistics were employed for all comparisons, with Bayes factors (BF_{10}) reported. Evidence categorized as moderate in favor of the null hypothesis (BF_{10} = 1/10–1/3), inconclusive (BF_{10} = 1/3–3), or moderate in favor of the alternative hypothesis (BF_{10} = 3–10) was excluded. Instead, we collected evidence classified as strong (BF_{10} = 10–30), very strong (BF_{10} = 30–100), or decisive (BF_{10} > 100) to either support (H1: there is an effect) or reject (H0: there is no effect) each hypothesis.[24,25] t values and Bonferroni-corrected p derived from classical Student's t tests were reported to complement Bayesian statistics.

In the sleep dataset, Bayesian independent sample t tests (two-tailed) yielded decisive evidence for lVPL reduction, strong

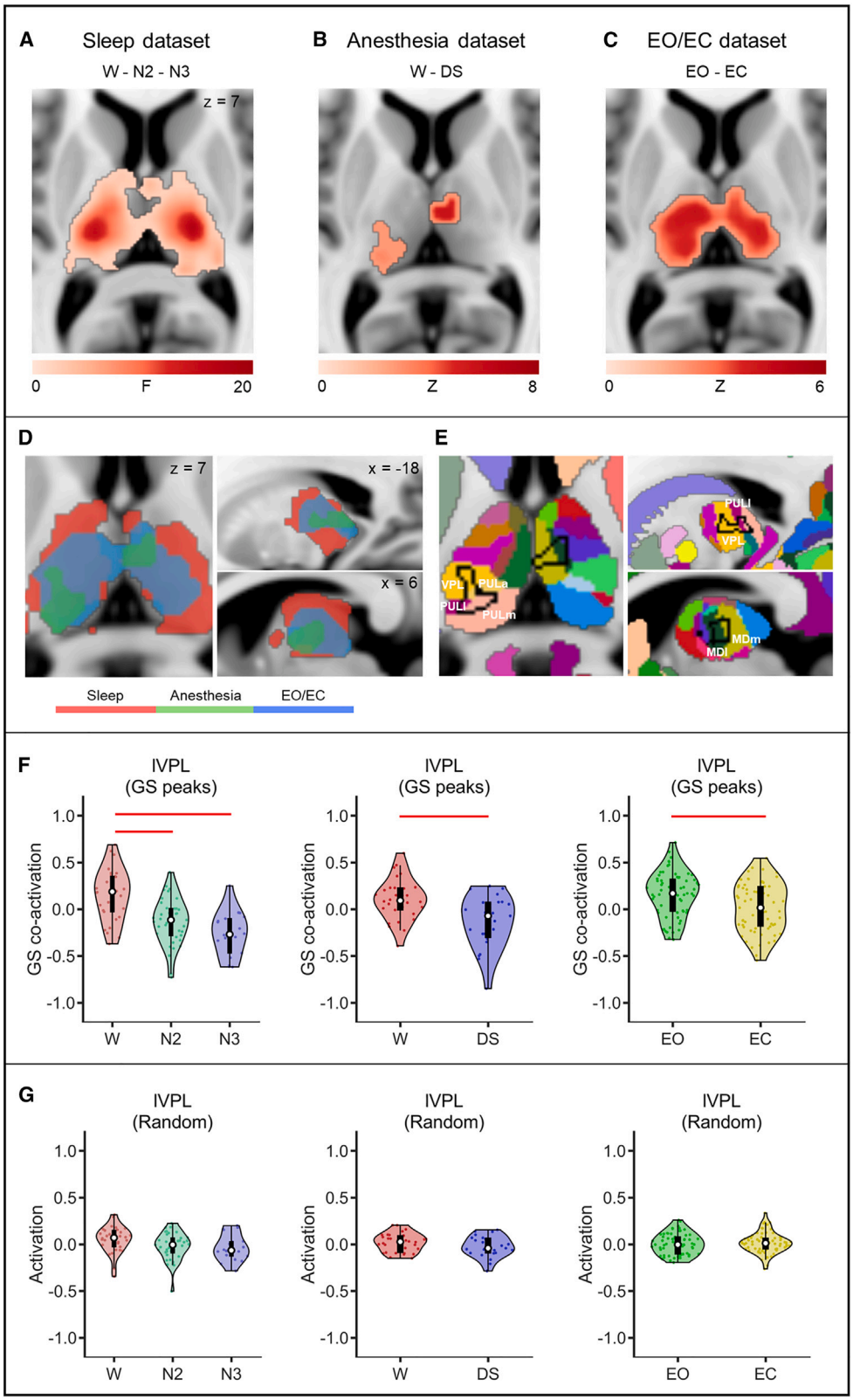

(legend on next page)

evidence for lPUL reduction, and moderate evidence for rMD reduction during both N2 (lVPL: BF_{10} = 613.513, t = 4.475, p = 0.002; lPUL: BF_{10} = 17.956, t = 3.238, p = 0.011; rMD: BF_{10} = 4.8662, t = 2.6767, p = 0.0564) and N3 sleep (lVPL: BF_{10} = 6103.452, t = 5.402, p < 0.001; lPUL: BF_{10} = 17.427, t = 3.274, p = 0.002; rMD: BF_{10} = 5.7092, t = 2.7648, p = 0.049) relative to wakefulness. Comparisons between N2- and N3-sleep stages showed inconclusive evidence for lVPL and lPUL alterations and moderate evidence for rMD changes (lVPL: BF_{10} = 1.230, t = 1.904, p = 0.374; lPUL: BF_{10} = 0.378, t = 0.824, p = 1.000; rMD: BF_{10} = 0.324, t = 0.551, p = 1.000) (Figures 2F and S1A; Data S1 and S2). To assess distinct activation pattern at GS peaks, we compared nucleus activation at random time points across stages. No strong evidence for reduced activation was found in any of the nuclei (Figures 2G and S1B; Data S3 and S4), and no strong evidence for altered GS co-activation was found in the physiological noise, including white matter (WM) or cerebral spinal fluid (CSF), among sleep stages (Figure S1C; Data S1 and S2), ruling out the possibility that the GS co-activation changes in the nuclei were contributed by these noise signals.

In the anesthesia dataset, Bayesian independent sample t tests (two-tailed) revealed very strong evidence for reduction in the lVPL, lPUL, and rMD during deep sedation relative to wakefulness (lVPL: BF_{10} = 33.207, t = 3.518, p = 0.006; lPUL: BF_{10} = 40.046, t = 3.592, p = 0.004; rMD: BF_{10} = 39.638, t = 3.588, p = 0.005) (Figures 2F and S2A; Data S1 and S2). No strong evidence for reduced activation at random time points was found in any nuclei (Figures 2G and S2B; Data S3 and S4), and there was no strong evidence for reduced GS co-activation in physiological noise (i.e., WM and CSF) (Figure S2C; Data S1 and S2).

In the resting-state EO/EC dataset, Bayesian paired sample t tests (two-tailed) yielded decisive evidence for reductions in all three nuclei from EO to EC (lVPL: BF_{10} = 141.212, t = 4.015, p < 0.001; lPUL, BF_{10} = 1080.326, wakefulness [W] = 1830, p = 0.001, non-parametric test due to violated parametric test assumption; rMD: BF_{10} = 149.753, t = 4.034, p < 0.001) (Figures 2F and S3A; Data S1 and S2). No strong evidence was found for reduced activation at random time points in any nuclei (Figures 2G and S3B; Data S3 and S4). Additionally, no strong evidence emerged for GS co-activation changes attributable to physiological noise (Figure S2C; Data S1 and S2).

Overall, the results indicated consistent reductions in GS co-activation for lVPL and lPUL across deep sleep, deep sedation, and EC conditions, while rMD exhibited reductions solely in deep sedation and EC conditions. These findings suggest a potential association between lVPL and lPUL global transient co-activation with arousal, while rMD co-activation appears less tightly linked.

Given the simultaneous decline in both arousal and awareness during sleep, anesthesia, and EC states, it is crucial to dissociate the distinct roles of thalamic nucleus-global transient co-activation in arousal vs. awareness. To this end, we included patients with UWS, characterized by high arousal but lack of awareness, and individuals in REM sleep, marked by high awareness (i.e., rich subjective experience) but diminished arousal.[1] We aimed to investigate whether thalamic nucleus-global transient co-activation predominantly associates with arousal by comparing UWS to wakeful controls, REM to wakefulness, REM to N3 sleep, and UWS to N3 sleep. Our hypothesis posits that if global transient co-activation primarily relates to arousal rather than awareness, it should persist in patients with UWS similarly to wakeful controls (both exhibiting high arousal), as well as in REM sleep akin to N3 sleep (both featuring low arousal). Conversely, we anticipate a reduction in REM sleep compared to wakefulness, as arousal decreases in REM sleep while awareness remains high in both conditions, and a lower level of co-activation in N3 sleep relative to patients with UWS due to the lower arousal levels in N3 sleep and reduced awareness in both states. Subsequent analyses will examine GS co-activation alterations in each nucleus in these comparative conditions.

For UWS patient comparisons, we recruited two datasets from Shanghai Hospital (SHH) and Zhujiang Hospital (ZJH), selecting only patients with UWS with well-preserved brain structures to mitigate structural distortion effects.[7] The SHH dataset included patients with UWS and brain injury (BI) with full conscious, while the ZJH dataset comprised patients with UWS and healthy controls (HCs) (Table 1). To test our hypothesis, GS co-activation was averaged within each thalamic nucleus (lVPL, lPUL, and rMD) (Figure 2E), and Bayesian independent sample t tests (two-tailed) were used to compare co-activation between UWS and BI in the SHH dataset, as well as between UWS and HCs in the ZJH dataset. The results showed inconclusive evidence for altered GS co-activation across all nuclei between UWS and BI (lVPL: BF_{10} = 0.6148, t = −1.279, p = 1.000; lPUL: BF_{10} = 0.3799, t = 0.601, p = 1.000; rMD: BF_{10} = 0.540, t = 1.130, p = 1.000) (Figures 3A and S4A; Data S1 and S2), and we found inconclusive evidence for lVPL and lPUL alterations and moderate evidence for rMD changes between UWS and HCs (non-parametric test due to violated parametric test assumption; lVPL: BF_{10} = 0.925, W = 135, p = 0.498; lPUL: BF_{10} = 1.675, W = 123, p = 0.231; rMD: BF_{10} = 0.322, W = 190, p = 1.000) (Figures 3B and S5A; Data S1 and S2). Furthermore, no strong evidence was found for the altered activation at random time points in any nuclei between conditions in either dataset (Figures 3A, 3B, S4B, and S5B; Data S3 and S4), nor for GS co-activation changes due to physiological noises (Figures S4C and S5C; Data S1 and S2).

For REM sleep comparison, we utilized sleep dataset 2 from our study, encompassing REM sleep, N3-sleep, and wakeful stages (Table 1). Bayesian independent sample t tests (two-tailed) were

Figure 2. Decreased GS co-activation in lVPL across reduced arousal states

(A–C) Comparison of GS co-activation maps between conditions in sleep, anesthesia, and EO/EC datasets (FDR-corrected $q < 0.05$).

(D) Overlapped thalamic region identified by intersecting the resulting brain maps from the above three datasets.

(E) Identification of specific thalamic nuclei, including lVPL, lPUL, and rMD, within the intersected region. Black line indicates the overlap from (D).

(F and G) Comparison of lVPL activation at GS peaks and random time points across conditions. Red line indicates BF_{10} >10. White dot denotes median value, box boundaries denote upper and lower quartiles, and whiskers denote 1.5× interquartile range. Sleep dataset: n_W = 30, n_{N2} = 37, n_{N3} = 18; anesthesia dataset: n_W = 30, n_{DS} = 23; EO/EC dataset: n_{EO} = 67, n_{EC} = 67.

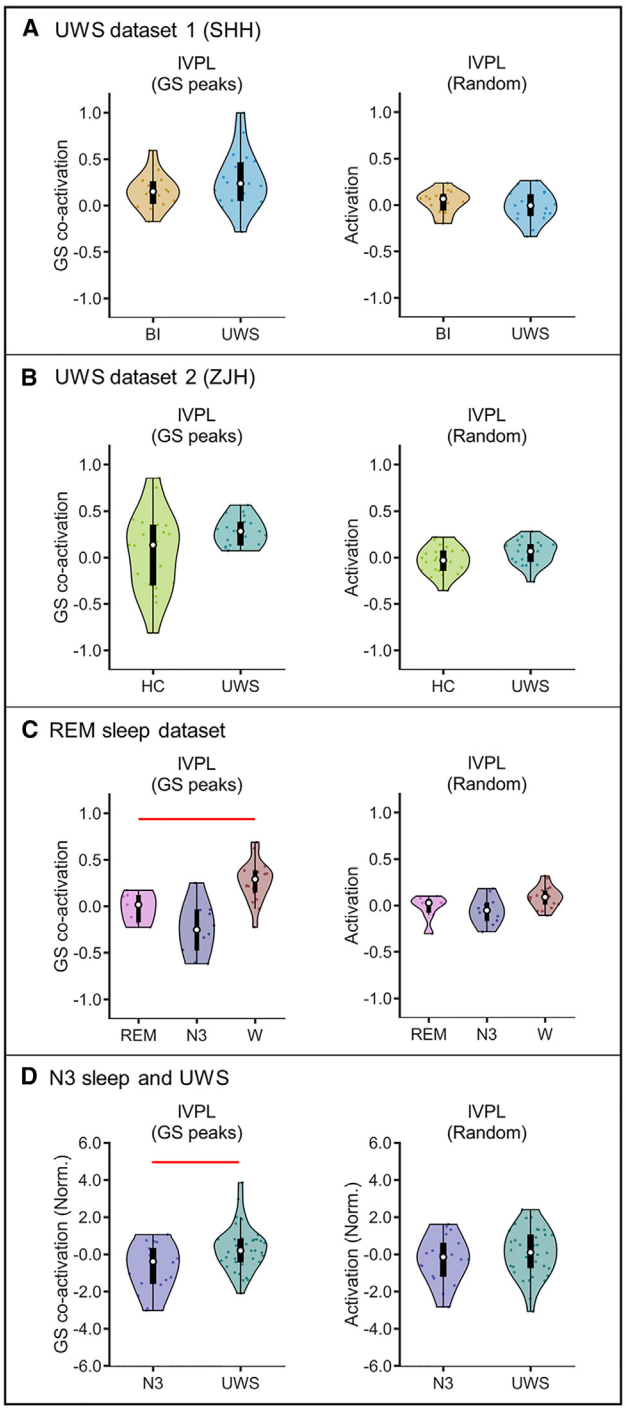

Figure 3. Comparative lVPL activation at GS peaks and random time points in states with dissociated arousal and awareness

(A) BI vs. UWS in UWS dataset 1 (SHH).

(B) HC vs. UWS in UWS dataset 2 (ZJH).

(C) REM vs. N3 vs. wakefulness (W) in sleep dataset 2. Another sleep dataset without REM sleep shows a similar lVPL activation contrast between W and N3 (Figure S10).

(D) N3 sleep vs. UWS, integrating data from both sleep datasets and UWS datasets, where activation values are normalized to control group, with age included as covariate in the contrast. Red line indicates BF_{10} >10. White dot denotes median value, box boundaries denote upper and lower quartiles, and whiskers denote 1.5× interquartile range. UWS dataset 1 (SHH): n_{BI} = 15, n_{UWS} = 19; UWS dataset 2 (ZJH): n_{HC} = 21, n_{UWS} = 19; REM sleep dataset: n_{REM} = 7, n_{N3} = 10, n_{W} = 19; N3 sleep and UWS: n_{N3} = 18, n_{UWS} = 36.

employed to compare average GS co-activation within each thalamic nucleus between REM and N3 sleep. Results yielded inconclusive evidence for alterations in lVPL and rMD and moderate evidence for lPUL (lVPL: BF_{10} = 1.411, t = 1.952, p = 0.419; lPUL: BF_{10} = 3.130, t = 2.587, p = 0.124; rMD: BF_{10} = 0.598, t = 1.014, p = 1.000) (Figures 3C and S6A; Data S1 and S2). No strong evidence was found for altered activation at random time points in any nuclei (Figures 3C and S6B; Data S3 and S4), nor for GS co-activation changes due to physiological noise (Figure S6C; Data S1 and S2).

Crucially, we examined GS co-activation across three thalamic nuclei between REM sleep and wakefulness, employing Bayesian independent sample t tests (one-tailed) to assess hypothesized reductions in REM sleep relative to wakefulness. The results showed strong evidence for a reduction in REM sleep in lVPL (BF_{10} = 19.040, t = −3.164, p = 0.013) but not in lPUL (BF_{10} = 1.994, t = −1.720, p = 0.295) or rMD (BF_{10} = 5.868, t = −2.476, p = 0.062) (Figures 3C and S6A; Data S1 and S2). No strong evidence was found for altered activation at random time points across the nuclei (Figures 3C and S6B; Data S3 and S4), nor for GS co-activation changes due to physiological noise (Figure S6C; Data S1 and S2).

For the comparison between N3-sleep and UWS conditions, we collected participants from two sleep and two UWS datasets in our study (Table 1). To reduce scanner-site variability, GS co-activation within each nucleus was *Z* score normalized relative to wakeful controls for each dataset. In brief, GS co-activation for each participant during N3 sleep (or UWS) was normalized by subtracting the mean of the control group and dividing by its standard deviation. Bayesian independent sample t tests (one-tailed) were employed to assess our hypothesis of lower GS co-activation in N3 sleep compared to UWS. The results showed strong evidence for a reduction in N3 in lVPL (BF_{10} = 13.849, t = −2.850, p = 0.019) but not in lPUL (non-parametric test due to violated parametric test assumption; BF_{10} = 0.577, W = 266, p = 0.883) or rMD (non-parametric test due to violated parametric test assumption; BF_{10} = 0.393, W = 308, p = 1.000) (Figures 3D and S7A; Data S1 and S2). No strong evidence was found for altered activation at random time points in any nuclei (Figures 3D and S7B; Data S3 and S4), nor for GS co-activation changes due to physiological noise (Figure S7C; Data S1 and S2). In addition, the spatial similarity of whole-brain functional connectivity patterns in controls from the UWS datasets was more akin to those observed during wakefulness than during N3 sleep in the sleep dataset (Figure S9; Table S1). This suggests a greater likelihood of wakefulness in the control group.

These results demonstrated that among the three thalamic nuclei, only the lVPL nucleus showed similar levels of transient global co-activation between patients with UWS and wakeful controls, as well as between REM and N3 sleep. Moreover, reduced co-activation was observed in REM sleep compared

to wakefulness and in individuals with N3 sleep compared to patients with UWS. These findings supported our hypothesis, suggesting that VPL-global co-activation is predominantly related to arousal rather than awareness.

Furthermore, considering the predominant relation with arousal found in the lVPL, we investigated whether the right VPL (rVPL) nucleus exhibited similar results. To address this, we defined a spherical region with a radius of 4 mm (MNI [Montreal Neurological Institute] coordinates: x = 18, y = −21, z = 6) based on the center coordinate of the lVPL (x = −18, y = −21, z = 6). The rVPL was then used as the ROI to replicate all previous analyses regarding GS co-activation and activation at random time points.

The results demonstrated that the majority of findings in the lVPL were replicable in the rVPL, albeit with minor variances. Specifically, decisive evidence (BF_{10} > 100) was identified for reduced GS co-activation in both N2 sleep and N3 sleep compared to wakefulness, whereas inconclusive evidence (BF_{10} = 0.7254) was observed for alterations between N2 and N3 sleep. Decisive evidence was also found when comparing EC and EO conditions. Inconclusive evidence was found between patients with UWS and wakeful controls across two datasets (SSH, BF_{10} = 0.5465; ZJH, BF_{10} = 0.4646). Decisive evidence was found for a reduction in REM sleep compared to wakefulness, while inconclusive evidence (BF_{10} = 0.6626) for alteration was observed between REM and N3 sleep. Contrarily, we found inconclusive evidence in deep sedation compared to wakefulness (BF_{10} = 1.0357) and moderate evidence in participants during N3 sleep relative to patients with UWS (BF_{10} = 4.4257), diverging from findings in the lVPL. Note that the reduction in the rVPL during sleep and EC conditions, as well as the absence of alteration during deep sedation, was consistent with the voxel-wise result (Figures 2A–2C). Additionally, no strong evidence was found for activation at random time points in each paired comparison. These results are presented in Figure S8, and detailed statistics are provided in Data S1, S2, S3, and S4.

DISCUSSION

In summary, our study reveals a pronounced elevation in VPL thalamic activation during transient GS peaks under states of elevated arousal compared to reduced arousal (e.g., wakefulness vs. N2/N3 sleep, wakefulness vs. deep sedation, EO vs. EC, REM sleep vs. wakefulness, and N3 sleep vs. UWS). This suggests that the co-activation between the VPL and the whole cortex is related to arousal in a general way. Importantly, when examining conditions that dissociate arousal and awareness, such as UWS (high arousal, low awareness) and REM sleep (low arousal, high awareness), we found that high VPL activation during GS peaks predominantly correlates with arousal rather than awareness.

Our findings are in line with previous animal studies that have demonstrated the modulatory role of sensory thalamic nuclei on cortical activity during quiet wakefulness and non-REM sleep.[17–19] Extending these previous findings, our study highlights the involvement of the sensory thalamic nucleus VPL in arousal. How does the VPL, a sensory thalamus nucleus receiving ascending input from the medial lemniscus and projecting to the somatosensory cortex,[26,27] affect widespread cortical activity to modulate arousal states? A recent study provided insights by suggesting that the sensory-motor regions could drive spontaneous large-scale cortical activity switching between high and low coherent states.[20] Moreover, a recent theory of sleep-wake control proposed an intimate association between arousal system and somatic motor control circuits.[28] Combining these findings with our results, it is plausible that the VPL achieves co-activation with large-scale cortical regions through the sensory-motor regions, thereby implementing arousal modulation. Although both the current results and some previous findings have proposed that the GS reflected brain-wide (or global) fluctuations in resting BOLD signals and carried neurophysiological information,[22,29,30] other studies have viewed GS as a physiological and head-motion noise.[31,32] To address this concern, we conducted control analyses to rule out the potential confounding effects from these noises (Figures S1, S2, S3C, and S4).

In the current study, GS co-activation of VPL remained comparable between UWS and fully conscious states (i.e., HC and BI) but was reduced during REM sleep compared to wakefulness. These results suggest that the transient co-activation between the VPL and GS is predominantly associated with arousal, rather than awareness, as patients with UWS exhibit high arousal without awareness and REM sleep involves low arousal with high awareness.[1] In addition to the previously found high brain stem activation[2] and specific electroencephalogram (EEG) features of arousal in UWS,[33] our findings showed that connections between subcortical structures and the cortex could be generally related to arousal, especially the arousal state in UWS. Notably, this result was also different from previous animal studies, in which activation of non-sensory thalamic nuclei induced widespread cortical activity in anesthetized or sleeping monkey and mice, leading to the recovery of consciousness (both arousal and awareness).[14,15,34,35] In these animal studies, targets in the thalamus included the central lateral thalamus (CL), the central thalamus (CT), the centromedial thalamus (CMT), and the paraventricular thalamus (PVT), all of which receive input from the brain stem reticular activating system and project to widespread cortical regions. Moreover, a human study showed that the stimulation of the CT could improve awareness in patients with disorders of consciousness.[16] However, these previous studies primarily focused on the relationship between non-sensory thalamic nuclei and the large-scale cortical regions in supporting consciousness (both arousal and awareness) rather than arousal alone.

Furthermore, contrary to the positive relationship between thalamic nuclei and the neocortex found in the current study and the above-mentioned studies, a recent study reported that the GS transient peaks co-occurred with the deactivation in the dorsal midline thalamus and the nucleus basalis, suggesting that the GS peaks were related to the momentarily reduced arousal.[13] This activity pattern is commonly found during microsleep state[10,36–38] or the transition from wakefulness to anesthesia,[39] and it is proposed to reflect the cortical activity's attempt to prevent a drop in awareness or arousal.[37] Considering the dynamic contribution of different cortical regions to the GS[40,41] and the diverse relationship between the thalamic nuclei

and the GS, it is likely that the global activity, VPL, and non-sensory thalamic nuclei function together in a complex manner to support arousal and normal consciousness. These findings call for further investigations to gain a deeper understanding in the future.

Limitations of the study

This study has several limitations. Firstly, while encompassing diverse arousal states—including sleep, deep sedation, EO/EC, and UWS—there remains a need to explore VPL-global co-activation in other alternative states, such as those induced by sleep deprivation,[42] caffeine consumption,[36] or variations in arousal as gauged by eyelid behavior or pupil dilation.[10,43] Moreover, the absence of direct interventions to modulate arousal level renders the relationship between VPL-global co-activation and arousal correlational rather than causal. Although this issue could be addressed by comparing sedated and non-sedated patients with UWS,[44] this experiment is challenging due to the individualized nature of clinical sedation protocols, and therefore it is more suitable for future investigations. Finally, the assumption that controls in the UWS datasets were fully awake is questioned by evidence indicating that some individuals may fall asleep during resting-state scans.[45] While we have demonstrated that controls were more likely to be in a wakeful state rather than in N3 sleep (Figure S9), future studies should incorporate real-time monitoring of participant arousal, particularly in research focusing on arousal states.

Conclusion

In conclusion, our study revealed that the higher activation in the VPL nucleus during transient peaks of GS is predominantly related to arousal, shedding light on our understanding of the neural correlates of arousal and consciousness. The predominant relationship observed between the VPL and arousal suggests a possibility that the electrical stimulation targeting the sensory thalamic nucleus could potentially enhance the arousal level in anesthetized macaques without improving their awareness. This approach may offer a promising animal model for UWS and the exploration of options for the diagnosis and treatment of disorders of consciousness.

STAR★METHODS

Detailed methods are provided in the online version of this paper and include the following:

- KEY RESOURCES TABLE
- RESOURCE AVAILABILITY
  - Lead contact
  - Materials availability
  - Data and code availability
- EXPERIMENTAL MODEL AND STUDY PARTICIPANT DETAILS
- METHOD DETAILS
  - Participants and data acquisition
  - UWS dataset
- QUANTIFICATION AND STATISTICAL ANALYSIS

SUPPLEMENTAL INFORMATION

Supplemental information can be found online at https://doi.org/10.1016/j.celrep.2023.113633.

ACKNOWLEDGMENTS

This work was sponsored by grants from the National Natural Science Foundation of China (grants 32371098 and 31971032 to P.Q. and 82271224 to X.W.), the Key Realm R&D Program of Guangzhou (202007030005 to P.Q.), the Lingang Laboratory (grant no. LG202105-02-03 to X.W.), the Shanghai Science and Technology Development funds (no. 16JC1420100 to Y.M.), the Shanghai Municipal Science and Technology Major Project (no. 2018SHZDZX01 to Y.M.), the Natural Science Foundation and Major Basic Research Program of Shanghai (16JC1420100), the Canadian Institutes of Health Research (CIHR), the Michael Smith Foundation (EJLB-CIHR), the Hope for Depression Research Foundation (HDRF), and the 2022 Guangdong-Hong Kong-Macao Greater Bay Area Exchange Programs of SCNU. This research project was also supported by the HBP Joint Platform to G.N., funded by the European Union's Horizon 2020 Framework Program for Research and Innovation under the specific grant agreement no. 785907 (Human Brain Project SGA 2).

AUTHOR CONTRIBUTIONS

Conceptualization, J.H. and P.Q.; methodology, Q.X., X.W., Z.H., S.T., and S.F.; formal analysis, J.H.; investigation, Q.X., X.W., Z.H., S.T., and S.F.; resources, Q.X., X.W., Y.M., and A.G.H.; writing – original draft, J.H. and P.Q.; writing – review & editing, J.H., Z.H., S.T., S.F., A.G.H., H.W., G.N., Y.M., S.H., and P.Q.; funding acquisition, X.W., Y.M., G.N., and P.Q.

DECLARATION OF INTERESTS

The authors declare no competing interests.

Received: January 10, 2023
Revised: November 21, 2023
Accepted: December 14, 2023

REFERENCES

1. Laureys, S. (2005). The neural correlate of (un)awareness: Lessons from the vegetative state. Trends Cogn. Sci. *9*, 556–559.
2. Bernat, J.L. (2006). Chronic disorders of consciousness. Lancet *367*, 1181–1192.
3. Demertzi, A., Tagliazucchi, E., Dehaene, S., Deco, G., Barttfeld, P., Raimondo, F., Martial, C., Fernández-Espejo, D., Rohaut, B., Voss, H.U., et al. (2019). Human consciousness is supported by dynamic complex patterns of brain signal coordination. Sci. Adv. *5*, eaat7603.
4. Huang, Z., Zhang, J., Wu, J., Mashour, G.A., and Hudetz, A.G. (2020). Temporal circuit of macroscale dynamic brain activity supports human consciousness. Sci. Adv. *6*, eaaz0087.
5. Luppi, A.I., Craig, M.M., Pappas, I., Finoia, P., Williams, G.B., Allanson, J., Pickard, J.D., Owen, A.M., Naci, L., Menon, D.K., and Stamatakis, E.A. (2019). Consciousness-specific dynamic interactions of brain integration and functional diversity. Nat. Commun. *10*, 4616.
6. Stevner, A.B.A., Vidaurre, D., Cabral, J., Rapuano, K., Nielsen, S.F.V., Tagliazucchi, E., Laufs, H., Vuust, P., Deco, G., Woolrich, M.W., et al. (2019). Discovery of key whole-brain transitions and dynamics during human wakefulness and non-REM sleep. Nat. Commun. *10*, 1035.
7. Qin, P., Wu, X., Wu, C., Wu, H., Zhang, J., Huang, Z., Weng, X., Zang, D., Qi, Z., Tang, W., et al. (2021). Higher-order sensorimotor circuit of the brain's global network supports human consciousness. Neuroimage *231*, 117850.

8. Wong, C.W., Olafsson, V., Tal, O., and Liu, T.T. (2013). The amplitude of the resting-state fMRI global signal is related to EEG vigilance measures. Neuroimage *83*, 983–990.

9. Wong, C.W., DeYoung, P.N., and Liu, T.T. (2016). Differences in the resting-state fMRI global signal amplitude between the eyes open and eyes closed states are related to changes in EEG vigilance. Neuroimage *124*, 24–31.

10. Chang, C., Leopold, D.A., Schölvinck, M.L., Mandelkow, H., Picchioni, D., Liu, X., Ye, F.Q., Turchi, J.N., and Duyn, J.H. (2016). Tracking brain arousal fluctuations with fMRI. Proc. Natl. Acad. Sci. USA *113*, 4518–4523.

11. Tanabe, S., Huang, Z., Zhang, J., Chen, Y., Fogel, S., Doyon, J., Wu, J., Xu, J., Zhang, J., Qin, P., et al. (2020). Altered Global Brain Signal during Physiologic, Pharmacologic, and Pathologic States of Unconsciousness in Humans and Rats. Anesthesiology *132*, 1392–1406.

12. Orban, C., Kong, R., Li, J., Chee, M.W.L., and Yeo, B.T.T. (2020). Time of day is associated with paradoxical reductions in global signal fluctuation and functional connectivity. PLoS Biol. *18*, e3000602.

13. Liu, X., De Zwart, J.A., Schölvinck, M.L., Chang, C., Ye, F.Q., Leopold, D.A., and Duyn, J.H. (2018). Subcortical evidence for a contribution of arousal to fMRI studies of brain activity. Nat. Commun. *9*, 1–10.

14. Redinbaugh, M.J., Phillips, J.M., Kambi, N.A., Mohanta, S., Andryk, S., Dooley, G.L., Afrasiabi, M., Raz, A., and Saalmann, Y.B. (2020). Thalamus Modulates Consciousness via Layer-Specific Control of Cortex. Neuron *106*, 66–75.e12.

15. Tasserie, J., Uhrig, L., Sitt, J.D., Manasova, D., Dupont, M., Dehaene, S., and Jarraya, B. (2022). Deep brain stimulation of the thalamus restores signatures of consciousness in a nonhuman primate model. Sci. Adv. *8*, eabl5547.

16. Schiff, N.D., Giacino, J.T., Kalmar, K., Victor, J.D., Baker, K., Gerber, M., Fritz, B., Eisenberg, B., O'Connor, J., O'Connor, J., et al. (2007). Behavioural improvements with thalamic stimulation after severe traumatic brain injury. Nature *448*, 600–603.

17. Hughes, S.W., Cope, D.W., Blethyn, K.L., and Crunelli, V. (2002). Cellular Mechanisms of the Slow (<1 Hz) Oscillation in Thalamocortical Neurons In Vitro. Neuron *33*, 947–958.

18. Poulet, J.F.A., Fernandez, L.M.J., Crochet, S., and Petersen, C.C.H. (2012). Thalamic control of cortical states. Nat. Neurosci. *15*, 370–372.

19. David, F., Schmiedt, J.T., Taylor, H.L., Orban, G., Di Giovanni, G., Uebele, V.N., Renger, J.J., Lambert, R.C., Leresche, N., and Crunelli, V. (2013). Essential thalamic contribution to slow waves of natural sleep. J. Neurosci. *33*, 19599–19610.

20. Kong, X., Kong, R., Orban, C., Wang, P., Zhang, S., Anderson, K., Holmes, A., Murray, J.D., Deco, G., van den Heuvel, M., and Yeo, B.T.T. (2021). Sensory-motor cortices shape functional connectivity dynamics in the human brain. Nat. Commun. *12*, 6373.

21. Liu, X., and Duyn, J.H. (2013). Time-varying functional network information extracted from brief instances of spontaneous brain activity. Proc. Natl. Acad. Sci. USA *110*, 4392–4397.

22. Zhang, J., Huang, Z., Tumati, S., and Northoff, G. (2020). Rest-task modulation of fMRI-derived global signal topography is mediated by transient coactivation patterns. PLoS Biol. *18*, e3000733.

23. Huang, C.-C., Rolls, E.T., Feng, J., and Lin, C.-P. (2022). An extended Human Connectome Project multimodal parcellation atlas of the human cortex and subcortical areas. Brain Struct. Funct. *227*, 763–778.

24. Keysers, C., Gazzola, V., and Wagenmakers, E.-J. (2020). Using Bayes factor hypothesis testing in neuroscience to establish evidence of absence. Nat. Neurosci. *23*, 788–799.

25. Huang, Z., Mashour, G.A., and Hudetz, A.G. (2023). Functional geometry of the cortex encodes dimensions of consciousness. Nat. Commun. *14*, 72.

26. Prescott, S.A., and Ratté, S. (2017). Somatosensation and Pain. In Conn's Translational Neuroscience, P.M. Conn, ed. (Elsevier), pp. 517–539.

27. Warren, S., Capra, N.F., and Yezierski, R.P. (2017). The Somatosensory System I: Tactile Discrimination and Position Sense. In Fundamental Neuroscience for Basic and Clinical Applications, Fifth Edition, D.E. Haines and G.A. Mihailoff, eds. (Elsevier.), pp. 243–257.

28. Liu, D., and Dan, Y. (2019). A Motor Theory of Sleep-Wake Control: Arousal-Action Circuit. Annu. Rev. Neurosci. *42*, 27–46.

29. Turchi, J., Chang, C., Ye, F.Q., Russ, B.E., Yu, D.K., Cortes, C.R., Monosov, I.E., Duyn, J.H., and Leopold, D.A. (2018). The Basal Forebrain Regulates Global Resting-State fMRI Fluctuations. Neuron *97*, 940–952.e4.

30. Schölvinck, M.L., Maier, A., Ye, F.Q., Duyn, J.H., and Leopold, D.A. (2010). Neural basis of global resting-state fMRI activity. Proc. Natl. Acad. Sci. USA *107*, 10238–10243.

31. Power, J.D., Plitt, M., Laumann, T.O., and Martin, A. (2017). Sources and implications of whole-brain fMRI signals in humans. Neuroimage *146*, 609–625.

32. Fox, M.D., Snyder, A.Z., Vincent, J.L., Corbetta, M., Van Essen, D.C., and Raichle, M.E. (2005). The human brain is intrinsically organized into dynamic, anticorrelated functional networks. Proc. Natl. Acad. Sci. USA *102*, 9673–9678.

33. Lee, M., Sanz, L.R.D., Barra, A., Wolff, A., Nieminen, J.O., Boly, M., Rosanova, M., Casarotto, S., Bodart, O., Annen, J., et al. (2022). Quantifying arousal and awareness in altered states of consciousness using interpretable deep learning. Nat. Commun. *13*, 1064.

34. Gent, T.C., Bandarabadi, M., Herrera, C.G., and Adamantidis, A.R. (2018). Thalamic dual control of sleep and wakefulness. Nat. Neurosci. *21*, 974–984.

35. Ren, S., Wang, Y., Yue, F., Cheng, X., Dang, R., Qiao, Q., Sun, X., Li, X., Jiang, Q., Yao, J., et al. (2018). The paraventricular thalamus is a critical thalamic area for wakefulness. Science *362*, 429–434.

36. Falahpour, M., Chang, C., Wong, C.W., and Liu, T.T. (2018). Template-based prediction of vigilance fluctuations in resting-state fMRI. Neuroimage *174*, 317–327.

37. Poudel, G.R., Innes, C.R.H., Bones, P.J., Watts, R., and Jones, R.D. (2014). Losing the struggle to stay awake: Divergent thalamic and cortical activity during microsleeps. Hum. Brain Mapp. *35*, 257–269.

38. Ong, J.L., Kong, D., Chia, T.T.Y., Tandi, J., Thomas Yeo, B.T., and Chee, M.W.L. (2015). Co-activated yet disconnected-Neural correlates of eye closures when trying to stay awake. Neuroimage *118*, 553–562.

39. Kiviniemi, V.J., Haanpää, H., Kantola, J.H., Jauhiainen, J., Vainionpää, V., Alahuhta, S., and Tervonen, O. (2005). Midazolam sedation increases fluctuation and synchrony of the resting brain BOLD signal. Magn. Reson. Imaging *23*, 531–537.

40. Huber, R., Ghilardi, M.F., Massimini, M., and Tononi, G. (2004). Local sleep and learning. Nature *430*, 78–81.

41. Vyazovskiy, V.V., Olcese, U., Lazimy, Y.M., Faraguna, U., Esser, S.K., Williams, J.C., Cirelli, C., and Tononi, G. (2009). Cortical Firing and Sleep Homeostasis. Neuron *63*, 865–878.

42. Krause, A.J., Simon, E.B., Mander, B.A., Greer, S.M., Saletin, J.M., Goldstein-Piekarski, A.N., and Walker, M.P. (2017). The sleep-deprived human brain. Nat. Rev. Neurosci. *18*, 404–418.

43. Podvalny, E., King, L.E., and He, B.J. (2021). Spectral signature and behavioral consequence of spontaneous shifts of pupil-linked arousal in human. Elife *10*, e68265.

44. Kirsch, M., Guldenmund, P., Ali Bahri, M., Demertzi, A., Baquero, K., Heine, L., Charland-Verville, V., Vanhaudenhuyse, A., Bruno, M.A., Gosseries, O., et al. (2017). Sedation of patients with disorders of consciousness during neuroimaging: Effects on resting state functional brain connectivity. Anesth. Analg. *124*, 588–598.

45. Tagliazucchi, E., and Laufs, H. (2014). Decoding Wakefulness Levels from Typical fMRI Resting-State Data Reveals Reliable Drifts between Wakefulness and Sleep. Neuron *82*, 695–708.

46. Vahdat, S., Fogel, S., Benali, H., and Doyon, J. (2017). Network-wide reorganization of procedural memory during NREM sleep revealed by fMRI. Elife *6*, e24987.

47. Fang, Z., Ray, L.B., Owen, A.M., and Fogel, S.M. (2019). Brain activation time-locked to sleep spindles associated with human cognitive abilities. Front. Neurosci. *13*. 46–16.

48. Huang, Z., Liu, X., Mashour, G.A., and Hudetz, A.G. (2018). Timescales of intrinsic BOLD signal dynamics and functional connectivity in pharmacologic and neuropathologic states of unconsciousness. J. Neurosci. *38*, 2304–2317.

49. Kandeepan, S., Rudas, J., Gomez, F., Stojanoski, B., Valluri, S., Owen, A.M., Naci, L., Nichols, E.S., and Soddu, A. (2020). Modeling an auditory stimulated brain under altered states of consciousness using the generalized ising model. Neuroimage *223*, 117367.

50. Giacino, J.T., Kalmar, K., and Whyte, J. (2004). The JFK Coma Recovery Scale-Revised: Measurement characteristics and diagnostic utility. Arch. Phys. Med. Rehabil. *85*, 2020–2029.

51. Young, A.L., Marinescu, R.V., Oxtoby, N.P., Bocchetta, M., Yong, K., Firth, N.C., Cash, D.M., Thomas, D.L., Dick, K.M., Cardoso, J., et al. (2018). Uncovering the heterogeneity and temporal complexity of neurodegenerative diseases with Subtype and Stage Inference. Nat. Commun. *9*, 4273.

52. Power, J.D., Cohen, A.L., Nelson, S.M., Wig, G.S., Barnes, K.A., Church, J.A., Vogel, A.C., Laumann, T.O., Miezin, F.M., Schlaggar, B.L., and Petersen, S.E. (2011). Functional Network Organization of the Human Brain. Neuron *72*, 665–678.

53. Wu, H., Xie, Q., Pan, J., Liang, Q., Lan, Y., Guo, Y., Han, J., Xie, M., Liu, Y., Jiang, L., et al. (2023). Identifying patients with cognitive motor dissociation using resting-state temporal stability. Neuroimage *272*, 120050.

54. Huang, Z., Tarnal, V., Vlisides, P.E., Janke, E.L., McKinney, A.M., Picton, P., Mashour, G.A., and Hudetz, A.G. (2021). Asymmetric neural dynamics characterize loss and recovery of consciousness. Neuroimage *236*, 118042.

STAR★METHODS

KEY RESOURCES TABLE

REAGENT or RESOURCE	SOURCE	IDENTIFIER
Deposited data		
fMRI Anesthesia Dataset 2	Openneuro.org	https://openneuro.org/datasets/ds003171
fMRI EO/EC Dataset 1	Beijing Normal University	http://fcon_1000.projects.nitrc.org/indi/retro/BeijingEOEC.html
fMRI EO/EC Dataset 2	Beijing Normal University	http://rfmri.org/BeijingEOEC2_Raw
Activation of ROIs	Zenodo	https://doi.org/10.5281/zenodo.8356084
Software and algorithms		
AFNI	National Institutes of Health (NIH)	https://afni.nimh.nih.gov/
JASP (version 0.17.2.1)	https://jasp-stats.org/	https://jasp-stats.org/
Co-activation map	Zenodo	https://doi.org/10.5281/zenodo.8356084

RESOURCE AVAILABILITY

Lead contact

Further information and requests for resources and reagents should be directed to and will be fulfilled by the lead contact, Pengmin Qin (qin.pengmin@m.scnu.edu.cn).

Materials availability

This study did not generate new unique reagents.

Data and code availability

- The anesthesia fMRI dataset (Western University) and EO/EC fMRI dataset have been publicly available (https://openneuro.org/datasets/ds003171, http://fcon_1000.projects.nitrc.org/indi/retro/BeijingEOEC.html, http://rfmri.org/BeijingEOEC2_Raw). The source data for figures have been deposited at Zenodo and are publicly available as of the date of publication (https://doi.org/10.5281/zenodo.8356084).
- The code that supports the findings of this study has been deposited at Zenodo and is publicly available as of the date of publication (https://doi.org/10.5281/zenodo.8356084).
- Any additional information required to reanalyze the data reported in this work paper is available from the lead contact upon request.

EXPERIMENTAL MODEL AND STUDY PARTICIPANT DETAILS

Information on approvals for human experiments, and the demographic information of subjects can be found in each section below.

METHOD DETAILS

Participants and data acquisition

Sleep dataset

The sleep dataset consisted of two separate datasets that were combined to form a comprehensive dataset. The first dataset was acquired at Institut Universitaire de Gériatrie de Montréal (IUGM) and the other was at Western University. All participants who passed inclusion/exclusion criteria were instructed to sleep in the scanner over night with a simultaneous EEG-fMRI recording. After excluding the participants who had not enough continuous segments (90 fMRI volumes) in each sleep stage, we collected a total of 30 participants in wakefulness (12 male, age 25.06 ± 4.08), 37 participants in N2 sleep (15 male, age 25.30 ± 4.18), and 18 participants in N3 sleep (8 male, age 24.06 ± 4.07). Details about the participants and data acquisition of the two datasets were as follows.

Dataset1: IUGM

This dataset served as the basis for a published study[46]. Thirteen healthy right-handed adults (5 male, age 27.4 ± 3.6) passed the inclusion/exclusion criteria, and a simultaneous EEG-fMRI recording scan took place while subjects slept in the scanner. The sleep session was terminated when the maximum possible number of volumes for a single fMRI session (4000 volumes, lasting a maximum of 2.5 h) was reached, or if subjects voluntarily terminated the session. Ethical and scientific approval was obtained from the Research

Ethics Board at the IUGM, Montreal, Quebec, Canada and an informed written consent was obtained prior to entering the study. See the previous study for more detailed information about the participants criteria.[46]

Images were collected using a 3T TIM TRIO Siemens scanner with a 12-channel head coil. A structural volume was acquired in the sagittal plane using a magnetization prepared rapid gradient echo (MPRAGE) sequence: TR = 2300 ms, TE = 2.98 ms, FA = 9°, 176 slices, FoV = 256 × 256 mm2, voxel size = 1 × 1 × 1 mm3. For functional acquisitions, an echo-planar imaging (EPI) gradient echo sequence was used with the following parameters: TR = 2160 ms, TE = 30 ms, FA = 90°, FoV = 220 × 220 mm2, matrix size = 64 × 64, 40 transverse slices, slice thickness = 3 mm, 10% inter-slice gap, inplane resolution = 3.44 × 3.44 mm2. In order to minimize the effects of gradient artifact on electroencephalography recordings, the sequence parameters were chosen so that the MR scan repetition time (2160 ms) matched a common multiple of the EEG sample time (0.2 ms), the product of the scanner clock precision (0.1 ms) and the number of slices (40 slices). NREM periods and intermittent wakefulness periods were classified by the EEG scoring according to standard criteria of the American Academy of Sleep Medicine (AASM), and the longest continuous (at least 90 fMRI volumes) segments of sleep stages were selected to avoid discontinuities in our data analysis. After discarding subjects with insufficient data length of NREM or wakefulness periods, there remained 11 subjects for wakefulness, 12 subjects for N2 sleep, and 8 subjects for N3 sleep. See the previous study for more detailed information about the simultaneous EEG-fMRI data acquisition and EEG data preprocesssing.[46]

Dataset2: Western university

This dataset served as the basis for a published study[47]*. Twenty-seven healthy right-handed adults (10 male, age 23.76 ± 3.72) passed the inclusion/exclusion criteria and slept in the scanner with a simultaneous EEG-fMRI recording. For each participant, up to 2 h of sleep EEG–fMRI data were acquired. All study procedures and methods adhered to the Declaration of Helsinki and were approved by the Western University Health Science research ethics board. See the previous study for more detailed information about criteria.*[47]

Functional magnetic resonance imaging was performed at a 3.0T Magnetom Prisma MR imaging system (Siemens, Erlangen, Germany) using a 64-channel head coil. High-resolution anatomic images were acquired using a standard 3D Multislice MPRAGE sequence (TR = 2300 ms, TE = 2.98 ms, TI = 900 ms, FA = 9°, 176 slices, FoV = 256 × 256 mm2, matrix size = 256 × 256 × 176, voxel size = 1 × 1 × 1 mm3). During the sleep session, T2-weighted fMRI images were acquired with a gradient echo-planar imaging (EPI) sequence using axial slice orientation (TR = 2160 ms, TE = 30 ms, FA = 90°, 40 transverse slices, 3 mm slice thickness, 10% inter-slice gap, FoV = 220 × 220 mm2, matrix size = 64 × 64 × 40, voxel size = 3.44 × 3.44 × 3 mm3). An expert who was a registered polysomnographic technologist scored the EEG data acquired during the simultaneous EEG–fMRI sleep recordings according to standard criteria of the American Academy of Sleep Medicine (AASM). The longest continuous (at least 90 fMRI volumes) segments of sleep stages were selected to avoid discontinuities in our data analysis. After discarding subjects with insufficient data length of NREM or wakefulness periods, there remained 19 subjects for wakefulness, 25 subjects for N2 sleep, 10 subjects for N3 sleep, and 7 subjects for REM sleep. See the previous study for more detailed information about the simultaneous EEG-fMRI data acquisition and EEG data preprocesssing.*[47]

Anesthesia dataset

The anesthesia dataset consisted of two separate datasets that were combined to form a comprehensive dataset. The first dataset was obtained from the Medical College of Wisconsin, while the second dataset was an open dataset sourced from Western University. Participants with excessive head motion were excluded from the analysis, resulting in a final sample size of 30 participants during wakefulness and 23 participants during deep sedation. Detailed information regarding the participants and data acquisition procedures for each dataset is provided below.

Dataset1: Medical college of Wisconsin

This dataset served as the basis for a published study[48]*. A total of 15 healthy adults (9 male, age 26.73 ± 4.79) were included in this study. All subjects received four 15-min resting-state scans in wakefulness, propofol-induced light and deep sedation, and recovery. The OAAS (observer's assessment of alertness/sedation) was applied to measure the levels of behavioral responsiveness. During baseline conscious and recovery conditions, participants responded readily to verbal commands (OAAS score, 5). During light sedation, participants showed lethargic response to verbal commands (OAAS score, 4). During deep sedation, participants showed no response to verbal commands (OAAS score, 2 and 1). The corresponding target plasma concentrations vary across subjects (light sedation: 0.98 ± 0.18 μg/mL; deep sedation: 1.88 ± 0.24 μg/mL) because of the variability in individual sensitivity to anesthetics. The Institutional Review Board of Medical College of Wisconsin approved the experimental protocol.*

In this study, we combined the first half of wakefulness scan (first 7.5 min) and the second half of recovery scan (second 7.5 min) to generate a full conscious scan, which avoided the possible asleep state in a long resting state, and the unconscious state at the beginning of recovery. And we adopted the combined wakefulness and deep sedation scans in the current study. After excluding the subjects who had exceeding head motion, 14 subjects in wakefulness (8 male, age 26.57 ± 4.93) and 12 subjects in deep sedation (6 male, age 25.91 ± 4.70) remained.

Image data were acquired using a 3T Signa GE 750 scanner (GE Healthcare) with a standard 32-channel transmit/receive head coil. Functional imaging data were acquired using gradient-echo EPI images of the whole brain: 41 slices, TR/TE = 2000/25 ms, slice thickness = 3.5 mm, in-plane resolution = 3.5 × 3.5 mm; FOV = 224 mm, flip angle = 77°, image matrix: 64 × 64. High-resolution spoiled gradient-recalled echo anatomical images were acquired before the functional scans with parameters: TE/TR/TI, 8.2/3.2/450 ms, slice thickness = 1 mm, number of slices = 150, flip angle = 12°, field of view = 24 cm, matrix size = 256 × 256. More detail information about the experiment protocol and data acquisition parameters were shown in the previous study.[48]

Dataset2: Western university

The second dataset in the anesthesia study is publicly available on Openneuro.org (https://openneuro.org/datasets/ds003171). This dataset includes a total of 17 healthy participants (13 males, age 24 ± 5). Each participant underwent four 8.5-min resting-state scans (256 volumes) under different conditions: wakefulness, propofol-induced light sedation, propofol-induced deep sedation, and recovery. The propofol infusion was administered intravenously using a Baxter AS 50 (Singapore), and the infusion rate was adjusted to achieve the desired level of sedation, guided by the TIVA Trainer, a pharmacokinetic simulation program (developed by the European Society for Intravenous Anesthesia, eurosiva.eu). The level of consciousness was assessed using the Ramsey scale.

During the awake session, participants were fully awake, alert, and able to communicate appropriately. In the mild sedation phase, participants exhibited a decrease in spontaneous conversation, slowed speech, and responsiveness only to loud commands (Ramsey 3). The target concentration of propofol infusion for light sedation was set at 0.6 μg/mL. In the deep sedation phase, participants did not respond to verbal commands and could only be aroused by light physical stimulation (Ramsey 5). The target concentration of propofol infusion was increased in increments of 0.3 μg/mL until the desired level of sedation was reached, as assessed by responsiveness. Once a Ramsey score of 5 was achieved, the concentration was maintained. In the recovery phase, participants demonstrated clear and prompt responses to verbal commands (Ramsey 2). The study received ethical approval from the Health Sciences Research Ethics Board and Psychology Research Ethics Board of the University of Western Ontario. Written informed consent was obtained from all participants.

After excluding subjects with excessive head motion, the final dataset consisted of 16 subjects during wakefulness and 11 subjects during deep sedation. Unfortunately, due to privacy concerns, the demographic information of each participant is not provided on the OpenNeuro, and as a result, the age and gender of the remaining participants could not be calculated.

Image data were acquired using a 3 TT Siemens Tim Trio system with a 32-channel head coil. Functional imaging data were acquired using gradient-echo EPI images of the whole brain: 33 slices, TR/TE = 2000/30 ms, voxel size = 3 × 3 × 3 mm^3, inter-slice gap of 25%, flip angle = 75°, image matrix: 64 × 64. High-resolution spoiled gradient-recalled echo anatomical images were acquired with parameters: TE = 4.25 ms, voxel size = 1 × 1 × 1 mm^3, flip angle = 9°, matrix size = 240 × 256 × 192. More detail information about the experiment protocol and data acquisition parameters were shown in the previous study.[49]

EO/EC dataset

This dataset combined two open resting-state datasets, which were recruited from Beijing Normal University. All participants were instructed to rest with eyes open or eyes closed without falling asleep. After excluding the participants with incomplete image data, we obtained a total of 67 participants (34 male, age 22.04 ± 2.18) in this study. More information about the participants and data acquisition of these datasets were introduced in the following.

Dataset1: Beijing normal university 1

This dataset is recruited in Beijing Normal University, which is available on the NITRC (NeuroImaging Tools and Resources Collaboratory) Website (http://fcon_1000.projects.nitrc.org/indi/retro/BeijingEOEC.html). A total of 47 healthy participants (23 male, age 22.51 ± 2.17) were included after excluding one participant with incomplete data. None of these participants had a history of medical, neurological, or psychiatric disorders. Each participant received three resting-state fMRI scans and was instructed to keep as motionless as possible and not to engage in any systematic thinking. Each of these scans lasted for 8 min. During the first scan, each participant was instructed to rest with their eyes closed. The second and third resting-state scans consisted runs with both eyes open or closed, of which the order was counterbalanced across all participants. Immediately after each session, the experiment operator spoke briefly with the participants. All the participants reported that they had not fallen asleep during the scan. Only the second and third resting scans were used in this study.

The fMRI data were acquired on a 3T Siemens Trio TIM MR scanner using a gradient-echo EPI sequence: TR = 2000 ms, TE = 30 ms, flip angle = 90°, FOV = 200 × 200 mm2; matrix = 64 × 64; slice thickness/gap = 3.5/0.7 mm; 33 slices. A total of 240 volumes were acquired in each run (8 min). A high-resolution T1-weighted anatomical image was also acquired using the MP-RAGE sequence: 128 slices, TR = 2530 ms, TE = 3.39 ms, slice thickness/gap = 1.33/0 mm, flip angle = 7°, inversion time = 1100 ms, FOV = 256 × 256 mm2, and in-plane resolution = 256 × 192.

Dataset2: Beijing normal university 2

This dataset was recruited from Beijing Normal University, which is available on the NITRC (NeuroImaging Tools and Resources Collaboratory) Website (http://rfmri.org/BeijingEOEC2_Raw). A total of 20 healthy participants (10 male, age 20.95 ± 1.82) were included. None of these participants had a history of medical, neurological, or psychiatric disorders. The participants received four scans, including three resting-state and one visual response task. They first underwent an EC resting-state scan. The second and third resting-state scan were in EO and EO-F (EO with a fixation), respectively. These scans were counterbalanced across the participants. Each of these scans lasted for 8 min. During the three resting-state sessions, the participants were instructed to keep as motionless as possible and not to engage in any systematic thinking. Immediately after each scanning session, the experiment operator had a short communication with the participants. All participants reported that they had not fallen asleep during the scan. Only the scans of EC and EO were used in this study.

The fMRI data were acquired on a 3T Siemens Trio TIM MR scanner using an echo-planar imaging sequence with the following parameters: TR = 2000 ms; TE = 30 ms; flip angle = 90°; FOV = 200 × 200 mm; in-plane resolution = 64 × 64; slice thickness/gap = 3/0.6 mm; 33 slices. A total of 240 volumes were acquired in each run (8 min). In addition, a T1-weighted sagittal three-dimensional magnetization-prepared rapid gradient echo (MPRAGE) sequence was acquired, covering the entire brain: 128

slices, TR = 2530 ms, TE = 3.39 ms, slice thickness = 1.33 mm, flip angle = 7°, inversion time = 1100 ms, FOV = 256 × 256 mm2, and in-plane resolution = 256 × 192.

UWS dataset

The shanghai hospital dataset (SHH)

This dataset served as the basis for a published study[7]. We included 50 patients with structurally well-preserved brains under three conditions: UWS, MCS and BIwith full conscious and a brain injury history. These structurally well-preserved patients, who were selected by author XW and then checked by author PQ according to their structural images, had limited brain lesions and limited brain structure distortion. The UWS and MCS patients were assessed using the Coma Recovery Scale-Revised (CRS-R)[50] before the fMRI scanning. Two hundred fMRI volumes (∼6.7 min) were acquired during rest for each subject. All participants were given the same instructions, in which they were told to take a comfortable supine position, relax, close their eyes, and not concentrate on anything in particular during the scanning. Informed written consent was obtained from the patients' legal representatives. The study was approved by the Ethics Committee of Shanghai Huashan Hospital, Fudan University, Shanghai, China. In this study, only the UWS and BIpatients were included. After excluding the patients who had exceeding motions, 15 BIpatients (11 male, age 38.8 ± 16.89) and 19 UWS patients (14 male, age 45.84 ± 12.49) remained.

Image data were acquired on the same Siemens 3 Tesla scanner. Functional images were acquired using a T2-weighted EPI sequence: TR/TE/θ = 2000 ms/35 ms/90°, FOV = 256 × 256 mm, matrix = 64 × 64, 33 slices thickness = 4 mm, gap = 0 mm. A high-resolution T1-weighted anatomical image was also acquired for all participants with parameters: TE/TR = 2.98/2300 ms, slice thickness = 1 mm, matrix size = 256 × 256. More detailed information about the experiment protocol and data acquisition parameters were shown in the previous study.*[48]

The zhujiang hospital dataset (ZJH)

This dataset included 19 UWS patients (10 male, age 51.16 ± 11.57) with well-preserved brain structures and 21 healthy subjects (10 male, age 32.33 ± 10.42). The UWS patients were assessed using the Coma Recovery Scale-Revised (CRS-R)[50] before the fMRI scanning. Two hundred and forty fMRI volumes (∼8 min) were acquired during rest for each subject. All participants were given the same instructions, in which they were told to take a comfortable supine position, relax, and not concentrate on anything in particular during the scanning. Informed written consent was obtained from the patients' legal representatives. The study was approved by the Ethics Committee of Zhujiang Hospital, Guangzhou, China.

Image data were acquired on the same Philips 3 Tesla scanner. Functional images were acquired using a T2*-weighted EPI sequence: TR/TE = 2000 ms/30 ms, FOV = 224 × 224 mm2, matrix = 64 × 64, 33 slices thickness = 3.5 mm, gap = 0.7 mm. A high-resolution T1-weighted anatomical image was also acquired for all participants with parameters: TE/TR = 3.2/7 ms, slice thickness = 1 mm, matrix size = 256 × 256.

Data preprocessing

All MRI images of each dataset were processed using the AFNI software package (https://afni.nimh.nih.gov/). First, the first three volumes were excluded, followed by the elimination of spikes and the correction of slice timing. All functional images were registered to the base volume, which was considered to have minimum outliers. Both the anatomical and functional images were then aligned and registered to standard MNI space, and the spatial resolution of each voxel was resampled into $3mm^3$. Subsequently, the functional images were smoothed using a 6-mm full-width at half-maximum (FWHM) Gaussian kernel. The functional data were then band-pass filtered (0.01–0.1 Hz), and the nuisance factors (six demeaned motion parameters, first differences of six motion parameter, and five principal components of the signals from white matter and cerebrospinal fluid) were regressed out. Moreover, motion was quantified as the Euclidean norm calculated from the six motion parameters for 2 consecutive TRs, and a displacement of >0.4 mm was considered excessive. The volume at the corresponding time point of the excessive motion, as well as the preceding volume, were replaced by interpolated neighboring non-excessive volumes. Furthermore, volumes with >10% voxels of the base volume were flagged as outliers were also replaced with the interpolation method. Finally, the time series of each voxel was *Z* score transformed by subtracting its temporal mean and dividing by its temporal standard deviation.

GS co-activation analysis

The FSL software (https://fsl.fmrib.ox.ac.uk/fsl/fslwiki) was used to segment the anatomical image and obtained gray matter (GM) for each participant. The GS was extracted by averaging the *Z* score transformed signals within GM. The time points of the GS in the top 16.6% were selected to represent the instantaneous peaks.[13,22] Then the z-scored activation maps at these GS peak time points (top 16.6%) were averaged to generate the GS co-activation map.[13,21,22] (Figure 1B).

Voxel-wise GS co-activation comparison

To test our hypotheses, we performed voxel-wise comparisons of GS co-activation within the thalamus across different conditions. In sleep dataset. a voxel-wise one-way ANOVA (two-tailed) was performed on the GS co-activation within the thalamus, comparing wakefulness, N2 sleep and N3 sleep stages. Multiple comparisons were corrected using the false discovery rate (FDR) method.

In anesthesia dataset, a voxel-wise independent sample t test (two-tailed) was performed to compare the GS co-activation within thalamus between wakefulness and deep sedation. Scanner was included as a covariate to account for the two different types of scanners (Siemens and GE) used in the two datasets. FDR correction was used for the multiple comparisons.

In EO/EC dataset, voxel-wise paired sample t test (two-tailed) was performed to compare the GS co-activation within thalamus between EO and EC. FDR correction was used for the multiple comparisons.

Identification of thalamic nucleus

To identify the specific thalamic nuclei related to arousal, we overlapped the regions that showed GS co-activation differences among arousal levels from the previous experiments. The resulting overlapping thalamic sub-regions were further compared with the atlas of subcortical areas[23] to determine the specific thalamic nuclei involved. Several nuclei were found to be involved, including the lVPL, lPUL, and rMD. The combined regions covering left PULa, lPULi, lPULl, and lPULm were treated as lPUL, while the combined regions covering right MDl and MDm were considered as rMD in this study (Figure 2E).

Comparison of GS co-activation at thalamic nucleus between distinctive arousal levels

Utilizing Bayesian statistics via JASP (v0.17.2.1; https://jasp-stats.org/), we compared the GS co-activation of three nuclei across distinctive arousal states in sleep, anesthesia and EO/EC dataset. In the sleep dataset, Bayesian independent sample t-tests (two-tailed) were performed to compare GS co-activation between wakefulness and N2 sleep, wakefulness and N3 sleep, and N2 sleep and N3 sleep. In the anesthesia dataset, Bayesian independent sample t test (two-tailed) was used for the contrast between wakefulness and deep sedation, with the type of scanner included as covariate. In the EO/EC dataset, Bayesian paired sample t test (two-tailed) was used for the contrast between EO and EC.

Dissociating involvement of thalamic nucleus-global transient co-activation in arousal and awareness

To investigate the differential involvement of the thalamic nucleus-global transient co-activation in arousal and awareness, we first recruited fMRI data including UWS patients who exhibit with high arousal without awareness. Bayesian independent sample t-tests (two-tailed) were performed to compare the GS co-activation between UWS patients and BI individuals SHH dataset, as well as between UWS patients and HC in ZJU dataset.

Additionally, REM sleep, characterized by high awareness and diminished arousal, was also included in the study. Bayesian independent sample t-tests (two-tailed) was performed to compare GS co-activation between REM sleep and N3 sleep conditions. Furthermore, based on the assumption of lower arousal in REM sleep compared to wakefulness, Bayesian independent sample t-tests (one-tailed) were used to examine whether the GS co-activation of the nucleus was lower during REM sleep than during wakefulness.

To further investigate the differential influence of arousal changes, we compared GS co-activation between N3 sleep and UWS patients. Both conditions are characterized by unawareness but distinct arousal levels. However, these two conditions are collected from different datasets, raising concerns about systematic variation, such as protocols, image acquisition parameters and other intrinsic factors, that could confound the comparison. Although it is infeasible to eliminate the scanner-site effect, this bias could be reduced through a data normalization method prior to comparison. This method normalized the data relative to control group using z scores for each dataset, which was used in other imaging research[51]*. Specifically, within each dataset, the GS co-activation during N3 sleep in each participant was subtracted by the average GS co-activation during wakefulness across participants, and the resulting value was divided by the standard deviation of the GS co-activation during wakefulness across participants. Similarly, the GS co-activation of each nucleus in each UWS patient was subtracted by the average GS co-activation across wakeful controls, and the resulting value was divided by the standard deviation of the GS co-activation across controls. Subsequently, based on the assumption of a lower arousal in N3 sleep compared to UWS, Bayesian independent sample t test (one-tailed) was conducted to compare the GS co-activation between two conditions. Age of the participants was considered as a covariate in the contrast. Two outlier data points (*i.e., *larger than 3 standard deviations) were discarded in the UWS condition before the contrast.*

In addition, given the evidences that a proportion of control participants could fall asleep during resting-state scan,[45] we implemented an analytical approach to infer the arousal state of control subjects during MRI scanning. We hypothesized that the brain connectivity patterns of control subjects would more closely resemble those observed in the wakeful state than those in N3 sleep. To test this hypothesis, we computed ROI-based functional connectivity (FC) across entire brain for each control subject in UWS datasets. We then assessed the spatial similarity of these patterns to the averaged FC patterns observed during wakeful and N3 sleep states, respectively, and compared the spatial similarities between these two states.

In specific, we utilized a modified version of the functional atlas delineated by Power et al.,[52] incorporating adjustments based on recent studies,[48,53,54] to extract regional time series from 226 ROIs. This atlas has been applied to investigate functional network alteration among various state of arousal or consciousness state.[48,53,54] For each region within the atlas, we drew a sphere with a 5mm radius centered on the specified coordinates and derived regional time series by averaging the signal intensities of all voxels within each ROI. We then computed the FC between each pair of ROIs using Pearson correlation, thereby constructing a 226 × 226 FC matrix for each participant. These FC matrices were averaged across participants for both wakefulness and N3 sleep states. For each control subject in UWS dataset, we assessed the resemblance of their FC matrix to the averaged FC matrices of wakeful and N3 sleep by calculating the Pearson correlation coefficients of the vectorized FC from the upper triangular portion of the FC matrix. This yielded two sets of similarity scores—one for wakefulness and another for N3 sleep—which were then compared using a Bayesian paired sample t test (two-tailed). For the two sleep datasets and two UWS datasets included in this study, similarity analyses and comparisons were performed on four paired datasets, each comprising one sleep dataset and one UWS dataset: SHH and IUGM, SHH and WU, ZJH and IUGM, ZJH and WU. To further test the robustness of the result, we replicated the same analysis using extended Human Connectome Project (HCP) multimodal parcellation atlas, which included 421 ROIs from cortex and subcortical areas.[23]

Comparison for thalamic nucleus activation at random time points

To investigate whether the thalamic nucleus shows a distinctive relationship with arousal during GS peaks, the activation at random time points was examined. Random time points, equivalent in number to the time points in GS peaks (16.6% of the data length), were

selected, and their activation was averaged for each nucleus. The averaged activation at random time points was then compared between each paired conditions using the same statistical methods as in the group comparison for GS co-activation.

Comparison of GS co-activation at physiological noise

To assess the contribution of physiological noise, including white matter (WM) and cerebrospinal fluid (CSF), to GS co-activation, the GS co-activation of these noise signals was examined for alterations related to arousal levels. The masks of WM and CSF were generated by setting the threshold of 95% on tissue probability map in SPM toolbox. The GS co-activation within each mask was averaged for each participant, and comparisons were conducted between each paired condition using the same statistical methods as in the group comparison for GS co-activation.

Replication of the GS co-activation alteration among arousal level in right VPL

Considering the consistent alterations in GS co-activation observed in the left VPL across arousal levels, we further investigated if the right VPL would exhibit similar results. To address this, a spherical region with a 4-mm radius (MNI coordinate: x = 18, y = −21, z = 6) was drawn for the right VPL, based on the coordinates of the center of the left VPL (x = −18, y = −21, z = 6). The activation of the right VPL during GS peaks and at random time points was calculated for each condition, and all the comparisons among different arousal levels were replicated as in the left VPL.

QUANTIFICATION AND STATISTICAL ANALYSIS

All statistical analyses described in this paper were performed using AFNI for voxel-wise analysis and JASP for ROI analysis. Voxel-wise analyses included one-way ANOVA, independent sample t-tests, and paired sample t-tests (two-tailed) conducted using the AFNI programs 3dANOVA and 3dttest++. The resulting p values were corrected for multiple comparisons using FDR correction at a threshold of q = 0.05.

For ROI analysis, Bayesian statistic that implemented in JASP (v0.17.2.1; https://jasp-stats.org/) were used for the comparison between different arousal levels. Bayesian independent sample t-tests (two-tailed) were performed for the following activation comparison: wakefulness vs. N2 sleep, wakefulness vs. N3 sleep, N2 sleep vs. N3 sleep, wakefulness vs. deep sedation, BIvs. UWS, HC vs. UWS, and N3 sleep vs. REM sleep. Bayesian Paired sample t-testes (two-tailed) was performed for EO vs. EC in activation comparison, and W vs. N3 sleep in FC similarity comparison. Bayesian independent sample t test (one-tailed) was performed for two activation comparison: REM vs. wakefulness and N3 sleep vs. UWS. The results were reported with Bayes factors (BF_{10}) which represents p (data|H1: there is effect)/p (data|H0: there is no effect), along with posterior median with 95% credible interval (CI). The default effect size priors with Cauchy scale 0.707 was applied, and the strength of evidence was interpreted based on Jeffrey's criterion.[24] To minimize the false inference, we excluded moderate evidence in favor of the null hypothesis (BF_{10} = 1/10–1/3), inconclusive (BF_{10} = 1/3 - 3) or moderate evidence in favor of the alternative hypothesis (BF_{10} = 3–10). Instead, we collected strong (BF_{10} = 10–30), very strong (BF_{10} = 30–100), or decisive (BF_{10} > 100) evidence to either support (H1: there is effect) or reject (H0: there is no effect) either hypothesis.[24,25]

Classical t-tests that implemented in JASP were also used to complement Bayesian statistic in ROI analysis. All statistics in ROI analyses were replicated with Classical t-tests. The p value was Bonferroni corrected for multiple comparisons for each comparison, with a significance threshold set at $\alpha = 0.05$. Assumption checks were performed using the Shapiro-Wilk test for normality and Levene's test for homogeneity of variances. While most comparisons satisfied both data normality and equal variances, there were some cases that violated one of the two. In those instances, non-parametric tests were performed. Mann-Whitney U tests were applied for unpaired samples, and Wilcoxon signed-rank tests were applied for paired samples. The detailed statistics are provided in Data S1, S2, S3, and S4.